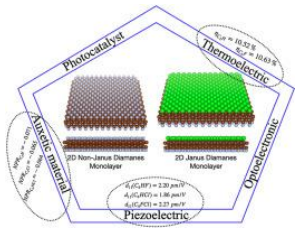


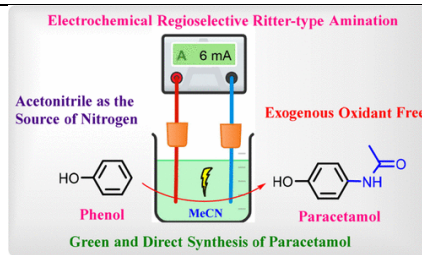
Sl. No.	<p style="text-align: center;">IIT Ropar List of Recent Publications with Abstract Coverage: March, 2022</p>
1.	<p>2D Janus and non-Janus diamanes with an in-plane negative Poisson's ratio for energy applications D Singh, N Khossossi, W Luo, A Ainane, R Ahuja - <i>Materials Today Advances</i>, 2022</p> <p>Abstract: Motivated by the successful synthesis of 2D C₂F diamanes [Bakharev, P.V. et al., <i>Nat. Nanotechnol.</i> 15, 59–66 (2020)], we have systematically investigated the structural stability, in-plane mechanical, optoelectronic, photocatalytic, piezoelectric, and thermoelectric properties of non-Janus and Janus diamanes monolayers named as C₂H, C₂F, C₂Cl, C₄HF, C₄HCl and C₄FCl. The structural stability is confirmed by cohesive energy, phonon dispersion spectra, and mechanical properties. The electronic properties has been calculated by HSE06 functional and the band gap are found to be 3.85, 5.64, 2.32, 4.16, 0.73 and 1.91 eV for C₂H, C₂F, C₂Cl, C₄HF, C₄HCl and C₄FCl, respectively. The hydrogen-containing non-Janus and Janus diamanes monolayers have a higher negative Poisson's ratio (NPR) and therefore are good auxetic materials. From the Poisson's ratio and Young's modulus of each configuration of non-Janus and Janus diamanes monolayer, anisotropic behavior was displayed. From the optical properties calculations, the refractive index values are around 1.5, which means that it will be a transparent monolayered materials. Also, C₂Cl, C₄HCl and C₄FCl monolayers displayed high absorption spectra with an order of 10⁵ cm⁻¹ in the visible region, which shows great applications in optoelectronic devices. Additionally, the valence and conduction band-edge positions of 2D Janus and non-Janus diamanes of C₂H, C₂F, and C₂Cl and C₄HF monolayers have to straddle the redox potentials of water. It means that the photogenerated electrons and holes are sufficient to drive the overall water splitting. Whereas non-Janus diamanes C₄HCl, and C₄FCl monolayers displayed only water oxidation. The investigated in-plane piezoelectric coefficient has larger in non-Janus diamanes C₄HF, C₄HCl, and C₄FCl monolayers. Therefore, it is very useful in the field of piezoelectric applications. From the thermoelectric properties, the non-Janus and Janus diamanes monolayers have great thermoelectric efficiency and were found to be 10.52 and 10.63% for C₂H and C₂F, respectively. Our results demonstrate the new class of 2D carbon-based monolayers has good auxetic materials as well as a wide range of applications in optoelectronics, piezoelectric, and thermoelectric fields.</p> <p>Graphical Abstract:</p>  <p>The graphical abstract illustrates the structural and functional properties of 2D Janus and non-Janus diamane monolayers. It shows two types of monolayers: a 2D Non-Janus Diamane Monolayer (left) and a 2D Janus Diamane Monolayer (right). The Janus monolayer is shown with a red top layer and a green bottom layer. The diagram is surrounded by labels for its various applications: Photocatalyst, Thermoelectric, Piezoelectric, and Auxetic material. Specific piezoelectric coefficients are listed: d₁₁(C₂H) = 3.22 pm/V, d₁₁(C₂F) = 1.96 pm/V, d₁₁(C₂Cl) = 3.22 pm/V, d₁₁(C₄HF) = 10.52 pm/V, and d₁₁(C₄HCl) = 10.63 pm/V.</p>
2.	<p>A characterization of weak proximal normal structure and best proximity pairs A Digar, RE García, GSR Kosuru - <i>Revista de la Real Academia de Ciencias Exactas, Físicas y Naturales. Serie A. Matemáticas</i>, 2022</p> <p>Abstract: The aim of this paper is to address an open problem given in [Kirk et al. in <i>J Math Anal Appl</i> 463:461–476, (2018)]. We give a characterization of weak proximal normal structure using best proximity pair property. We also introduce a notion of pointwise cyclic contraction wrt orbits</p>

	and therein prove the existence of a best proximity pair in the setting of reflexive Banach spaces.
3.	<p>A comprehensive study on the effect of line energy during laser bending of duplex stainless steel R Yadav, DK Goyal, R Kant - Optics & Laser Technology, 2022</p> <p>Abstract: Laser bending is a well-established process to achieve bending with high accuracy and good controllability. This study discusses the effect of line energy on bending mechanism, bend angle, edge effect, mechanical properties, and microstructural characterization for laser bending of duplex stainless steel. Numerical simulations have been carried out for a better understanding of the bending mechanisms. Additionally, the role of temperature distribution at the bottom surface on the variation in bend angle has been analyzed. It is found that at low laser powers, the bend angle increases with line energy, but at a decreasing rate. Whereas at high laser powers, the bend angle increases with line energy; attains peak and then decreases. At constant line energy, the bend angle increases with the increase in laser power and scanning speed. The hardness of laser-scanned specimens is increased, and ductility is reduced. Besides, the ultimate strength and yield strength remain almost constant. The sigma phase formation has been observed during the microstructural analysis, which further correlates with the high hardness and low ductility.</p>
4.	<p>A Fault-Tolerant Power Converter with Multi-Switch Fault Diagnosis and Repair Capability for 4-phase 8/6 SRM Drives AK Rana, AVR Teja - IEEE Transactions on Transportation Electrification, 2022</p> <p>Abstract: In this paper, a modular fault-tolerant power converter for 8/6 4-phase switched reluctance motor (SRM) drives is presented. The proposed converter can work for both open circuit and short circuit fault conditions in the power semiconductor switches. A semiconductor switch module and a relay circuit are used for achieving the fault tolerance feature. The proposed converter is modular and provides independent fault-tolerant control for all phases. It also uses minimum number of switches when compared with other fault-tolerant converter topologies. The proposed converter is tested for a fault in single as well as multiple phases using Matlab/Simulink software and is validated experimentally on a 0.6 hp 8/6 SRM using an FPGA-based hardware setup developed in the laboratory. Detailed results are presented and compared with existing fault-tolerant converter topologies. A fault repair time of 2 ms has been achieved for both open and short circuit faults.</p>
5.	<p>Analysis of ligaments formed during sheet atomization of non-Newtonian fluids AK Singh, KK Yadav, L Kabiraj, A Saurabh - Proceedings of the 26th National and 4th International ISHMT-ASTFE Heat and Mass Transfer Conference, 2021</p> <p>Abstract: The contribution deals with the analysis of sheet atomization of Carbopol-water gels. A like-on-like impinging jet configuration is employed. The breakup of the resulting sheet into ligaments and subsequently into droplets for a range of jet velocities and gel composition in these experiments has been recently reported in Saurabh et al. citeSaurabh2020, AIAA Propulsion and Energy, 2020. Here, the focus is on the analysis of ligaments and their breakup into children droplets. The ligaments shed from the sheet are investigated visually and quantitatively via image processing. A classification of sheet disintegration into ligaments into different breakup regimes and comparison with similar classification for Newtonian fluids has been reported. The analysis of ligament disintegration into droplets is based on the estimation of the roughness and uniformity of ligament structure separating from the main sheet. Predictions based on a theoretical framework for ligament disintegration have been compared with the distribution of children droplet sizes. Also reported is the distribution of the velocity of large-sized children droplets as a function of the azimuthal angle in the plane of the sheet for different gel concentrations and jet</p>

	<p>velocities.</p> <p>Application of delay embedding and recurrence analysis to a noisy nonlinear map for cyclic combustion dynamics of SI engines A Singh, RK Maurya - International Journal of Engine Research, 2022</p> <p>Abstract: A noisy nonlinear dynamical (NND) model available for cyclic variations in SI engines is examined using nonlinear time series methods. Heat release time series computed from this model is analyzed by employing bifurcation diagrams, return maps, recurrence plots, and recurrence quantitative analysis techniques. The analysis methodology is at first applied to a noisy Logistic map to optimize the necessary parameters, and later the same is used for the NND map. The presence of noise hides the local patterns of the dynamics and higher periodic orbits, making the bifurcation diagrams look fuzzy for both maps. An increase in the noise level and uncombusted residuals in the NND map advance the onset point of bifurcations toward a higher equivalence ratio. The application of the NND model is extended to represent the SI engine combustion dynamics for a higher amount of internal EGR as it is favored for cycle-resolved control due to its feedback period of one combustion cycle. The combined effect of lean charge and internal EGR leads to a more complex dynamical nature. The addition of a higher amount of internal EGR adds some complex chaotic-like regions in the bifurcation diagrams. For a low level of fluctuations in the NND map, more than four noisy periodic orbits are observed for such operating conditions. The geometry of phase space trajectories for the low-level noisy model data with a high level of internal EGR resembles a chaotic system. Bifurcation diagrams, recurrence plots, and quantitative recurrence analysis indicate an intermittent route to chaos at a highly lean and diluted charge. The presence of deterministic chaotic characteristics in combustion dynamics, along with effort-saving techniques of data acquisition and estimating combustion phasing, depicts the possibilities of practical application in active onboard control of engine systems.</p>
6.	<p>Assessing the effects of cost, revenue and profit efficiency on bank performance: empirical evidence from Indian banking B Rakshit - International Journal of Organizational Analysis, 2022</p> <p>Abstract: Purpose This paper aims to investigate the effects of cost, revenue and profit efficiency on bank profitability in an emerging economy such as India over the period 1997 to 2017. Additionally, this study examines the effect of efficiency on profitability across different ownership groups for a panel of 70 Indian commercial banks.</p> <p>Design/methodology/approach In the first stage, using stochastic frontier analysis, we estimate the efficiency scores of cost, revenue and profit over the examined period. In the second stage, this study uses the two-step system generalized-method of moments dynamic panel approach to investigate the impact of several efficiency measures on bank profitability.</p> <p>Findings Results estimated through and system generalized-method of moments indicate that a higher level of cost, revenue and efficiency significantly improves India's bank profitability. Regarding ownership groups, this study finds that the public sector banks are most cost-efficient compared to private and foreign banks. Other bank-specific, macroeconomic and institutional variables have played a significant role in determining bank profitability.</p>
7.	

	<p>Practical implications The findings of the study extend some important policy implications. In light of the rapid decline in bank profitability, banks should focus on increasing the efficiency of their operations. Improvement in profit, cost and revenue efficiency can ameliorate bank performance significantly. Profit efficiency that takes into account both cost and revenue efficiency should be maintained reasonably to prevent the declining pattern of bank profitability that the industry has witnessed over the years.</p> <p>Originality/value To the best of the author's knowledge, this study is a fresh piece of research that fulfils an urgent need of investigating the dynamics between bank efficiency and bank profitability in India. In an emerging economy like India, where the banking sector has witnessed substantial structural transformations over the past two decades, such study demands an immediate empirical investigation.</p>
8.	<p>Carnavalesque subversion and the narrative gaze of children: Taika Waititi's Boy (2010), Hunt for the Wilderpeople (2016), and Jojo Rabbit (2019) S Reji, A Nandha - Studies in Australasian Cinema, 2022</p> <p>Abstract: This article studies the carnivalesque subversion of oppressive systems using the narrative gaze of children in Taika Waititi's three films, Boy (2010), Hunt for the Wilderpeople (2016), and Jojo Rabbit (2019). Waititi has a wide range of filmography to his assets and his films, while comically articulating his politics, incorporate new vocabularies to tackle various forms of oppression. The selected films are of both local and international nature, and they voice their politics through the varying presence of carnivalesque motifs of subversion. The current paper attempts to investigate them using Bakhtin's theory of the carnivalesque. By arguing that these films are a vehicle of his personal and political credence, this paper attempts to bridge the gap in theorizing Waititi's filmography despite being critically acclaimed.</p>
9.	<p>Comparative Study of DGA Based Fault Diagnosis using ANN and Fuzzy Systems AH Kumar, B Singh, CC Reddy - Power Research, 2022</p> <p>Abstract: Dissolved Gas Analysis (DGA) method for fault detection has been implemented using Artificial Neural Networks (ANN), Fuzzy Logic (FL) and Adaptive Neuro Fuzzy Inference System (ANFIS). Incipient faults can be detected using DGA which provides reasonably good results. We have tried to improve this method in order to surpass its limitations. Comparative analysis using the mentioned methods have been done on IEC 599 standard, Rogers Ratio Method and Doernenburg's method. Using Fault databases, the training has been done to improve the diagnostic capabilities. The obtained results clearly show the superiority of ANFIS on ANN and FL. Being a combination of both, its degree of accuracy in prediction and ease of use, provides a promising alternative in replacing the conventional methods.</p>
10.	<p>Detection of abrupt change in trends of rainfall and rainy day's pattern of Uttarakhand S Rana, V Deoli, SR Chavan - Arabian Journal of Geosciences, 2022</p> <p>Abstract: Due to climate change, variations in rainfall and rainy days have significant effects on the hydrological cycle and these changes are important for planning and management of flood, drought, and water resources. The study aimed to determine spatio-temporal change in annual rainfall and rainy days for thirteen districts of Uttarakhand, India, located at the foothill of the Himalayan region. The temporal trend in data was determined using the Mann-Kendall (MK) test and the modified Mann-Kendall (MMK) test at a 10% level of significance after investigating</p>

	<p>autocorrelation in the data set using the student's t-test at a 10% level of significance. Theil's-Sen slope estimator test was used to evaluate the slope of rainfall and percentage change in rainfall over Uttarakhand. Furthermore, the sequential Mann-Kendal test (SMK) has been applied to determine the abrupt change in rainfall and rainy-day time-series. Results of the study show that six districts have an increasing trend from which two districts show a significant increasing trend and seven districts show a decreasing trend from which one district has a significantly decreasing trend at a 10% level of significance. In the case of rainy days, four districts have an increasing trend from which two districts show a significant increasing trend and nine districts show a decreasing trend from which no district show a significant decrease at a 10% level of significance. Based on the SMK test, Uttarkashi District shows a maximum of six change point years, whereas Rudraprayag District has no change point year in annual rainfall. For rainy days, Uttarkashi and U. S. Nagar Districts have a maximum of seven change point years, whereas Bageshwar, Haridwar, and Rudraprayag Districts have no change point years. Spatial distribution in annual rainfall and rainy days interpolated by inverse distance weighted (IDW) method in QGIS 3.14. The spatial map might be very helpful for local farmers, water managers, and stockholders to assess availability and risk of climate change in their region. The result of the study also could be very precious for agriculture planning, water management, and soil and water conservation for Uttarakhand.</p>
11.	<p>Direct Contact Membrane Distillation Coupled with Solar Collector: A Numerical Study D Chamoli, K Garg, H Tyagi - Proceedings of the 26th National and 4th International ISHMT-ASTFE Heat and Mass Transfer Conference, 2021</p> <p>Abstract: A numerical analysis of direct contact membrane distillation (DCMD), coupled with the solar collector for optimum performance is carried out. The working model of the system is defined mathematically, and numerical simulation is carried out for the same model. Nanofluid-based direct absorption solar collector (DASC) is used to heat water to the required feed temperature before it enters the DCMD. The presence of nanoparticles within the solar collector increases the absorption of incident solar irradiation compared to pure water. Various input parameters of module design such as depth of flow channel, and operating conditions like flow rate of feed, and membrane properties are varied to determine the optimum operating condition. Balancing the DCMD by keeping equal mass flowrate of feed and permeate in the membrane module (counter-current flow), recovering the waste permeate heat is performed. Results show that by flowrate balancing, there was a 15-30% increase in the performance of membrane distillation.</p>
12.	<p>Direct Synthesis of Paracetamol via Site-Selective Electrochemical Ritter-type C–H Amination of Phenol IM Taily, D Saha, P Banerjee - Organic Letters, 2022</p> <p>Abstract: The synthesis of paracetamol still relies on multistep protocols involving the utilization of a stoichiometric amount of oxidizing/reducing or other corrosive agents. Herein we report a regioselective electrochemical Ritter-type reaction at the C(sp²)-H of unprotected phenol toward the environmentally benign and direct synthesis of paracetamol. The reaction proceeds under exogenous oxidant- and catalyst-free conditions. The protocol is scalable, can be deployed to a variety of phenols, and offers a sustainable alternative for the synthesis of paracetamol.</p>



[Effect of collagen fibre orientation on the Poisson's ratio and stress relaxation of skin: an ex vivo and in vivo study](#)

KK Dwivedi, P Lakhani, S Kumar, N Kumar - Royal Society Open Science, 2022

13.

Abstract: During surgical treatment skin undergoes extensive deformation, hence it must be able to withstand large mechanical stresses without damage. Therefore, understanding the mechanical properties of skin becomes important. A detailed investigation on the relationship between the three-dimensional deformation response of skin and its microstructure is conducted in the current study. This study also discloses the underlying science of skin viscoelasticity. Deformation response of skin is captured using digital image correlation, whereas micro-CT, scanning electron microscopy and atomic force microscopy are used for microstructure analysis. Skin shows a large lateral contraction and expansion (auxeticity) when stretched parallel and perpendicular to the skin tension lines, respectively. Large lateral contraction is a result of fluid exudation from the tissue, while large rotation of the stiff collagen fibres in the loading direction explains the skin auxeticity. During stress relaxation, lateral contraction and fluid effluxion from skin reveal that tissue volume loss is the intrinsic science of skin viscoelasticity. Furthermore, the results obtained from in vivo study on human skin show the relevance of the ex vivo study to physiological conditions and stretching of the skin during its treatments.

[Effect of Power-Law Index and Shape on the Onset of Flow Separation](#)

G Mishra, RP Chhabra - Journal of Chemical Engineering of Japan, 2022

14.

Abstract: The present work investigates the first flow regime transition, namely, the onset of flow separation from the surface of a submerged body, for power-law fluids (shear-thinning and shear-thickening fluids) for a range of axisymmetric shapes. In particular, the geometries considered here include spheroids, hemisphere, spherical caps, cones, conical caps, frustum of cones and disks in two orientations with respect to the direction of the flow. Broadly, this transition occurs at progressively lower Reynolds numbers for objects with reduced degree of streamlining, or in the presence of geometric singularities (corners) and a high level of curvature, even in Newtonian fluids. The role of body shape is further accentuated for power-law fluids due to the variation in the fluid viscosity along the surface, as well as its spatial variation. For shear-thinning fluids ($n < 1$), the critical Reynolds number exhibits a peak somewhere around $n \sim 0.4-0.5$ for each shape studied here, and this is attributed to the interaction between the non-linear viscous and inertial forces prevailing in the flow field. For shear-thickening fluids, it progressively decreases with the increasing value of power-law index.

[Electronic bandstructure modulation of \$\text{MoX}_2/\text{ZnO}\$ \(X:S,Se\) heterostructure by applying external electric field](#)

NK Sharma, S Sahoo, MC Sahu, SK Mallik... R Ahuja... - Surfaces and Interfaces, 2022

15.

Abstract: The electronic properties of 2-Dimensional Van der Waals heterostructure of MX_2 (M:Mo, X:S, Se) and graphene-like ZnO by applying an external electric field (EF) in the range -0.50 V/\AA to 1.0 V/\AA is studied using first-principles calculations. The effect of the

	<p>transverse electric field is measured in terms of modulation of the electronic energy bandgap and change in the band alignment properties. The bandstructure of MoS₂/ZnO heterostructure(HS) shows an indirect bandgap of 1.61eV with a type-II band alignment and a large built-in electric field of 7.42eV with a valence band offset of 1.22eV across the interface. The bandstructure of MoSe₂/ZnO shows a direct bandgap of 1.81eV with type-I alignment and a built-in electric field of 3.64eV with a band offset of 0.31eV. The charge density is localized on MoS₂ and ZnO in VBM and CBM respectively in MoS₂/ZnO HS, whereas in MoSe₂/ZnO, both VBM and CBM are localized on MoSe₂. With a perpendicular electric field applied across the HS, re-alignment of bandstructure and modulation of bandgap in both the HSs occurs. The energy bandgap increases linearly with the applied electric field for MoS₂/ZnO(1.1–2.2eV) and remains almost constant(1.81eV) in the range -0.50V/Å to 0.50V/Å followed by a small decrease with an increase in electric field (1.60 for EF=±1.0V/Å). A cross-over in the bandgap type from indirect(type-II)→direct(type-I) in MoS₂-ZnO and direct(type-I) to indirect(type-II) in MoSe₂/ZnO has been observed at a critical value of electric field EF=0.75V/Å. The cross-over in band structure is consistent with the charge transfer pattern observed on the application of electric field. Tuning the electronic bandgap and changing the band-alignment with an external electric field opens a way to design futuristic electronic and optical devices.</p>
16.	<p>Entanglement degradation in multi-event horizon spacetimes S Bhattacharya, N Joshi - Physical Review D, 2022</p> <p>Abstract: We investigate the degradation of quantum entanglement in the Schwarzschild-de Sitter black hole spacetime, by studying the mutual information and the logarithmic negativity for maximally entangled, bipartite states for massless minimal scalar fields. This spacetime is endowed with a black hole as well as a cosmological event horizon, giving rise to particle creation at two different temperatures. We consider two independent descriptions of thermodynamics and particle creation in this background. The first involves thermal equilibrium of an observer with either of the horizons. We show that as of the asymptotically flat/anti-de Sitter black holes, in this case, the entanglement or correlation degrades with increasing Hawking temperatures. The second treats both the horizons combined in order to define a total entropy and an effective equilibrium temperature. We present a field theoretic derivation of this effective temperature and show that unlike the usual cases, the particle creation does not occur here in causally disconnected spacetime wedges but instead in a single region. Using the associated vacua, we show that in this scenario, the entanglement never degrades but increases with increasing black hole temperature and holds true no matter how hot the black hole becomes or how small the cosmological constant is. We argue that this phenomenon can have no analogue in the asymptotically flat/anti-de Sitter black hole spacetimes.</p>
17.	<p>Forced Convection from Chains of Spheres A Varma, P Suri, SA Patel - Proceedings of the 26th National and 4th International ISHMT-ASTFE Heat and Mass Transfer Conference, 2021</p> <p>Abstract: Operations involving clusters of particles moving together as agglomerates in fluid media are encountered in a plethora of industrial processes like drying operations, fluidized transportation, continuous thermal treatment of food stuff etc. to name a few. These agglomerates move through such fluids, affect the flow field and in turn, are affected by it in ways different than in the case of an individual particle. The present study is an idealization of the aforementioned situation in which a linear chain of heated spheres ($1 \leq N \leq 20$) is moving in a pool of air ($Pr = 0.72$) in laminar steady state flow ($1 \leq Re \leq 100$) conditions. The governing mathematical equations have been solved numerically employing finite element methodology subjected to appropriate boundary conditions. The effect of number of spheres in chain (N) as well as flow</p>

	<p>conditions (Re) on the hydrodynamics and thermal behaviour of the flow have been studied in detail. Developed flow field with increasing Re has been visualized by mapping vorticity contours and streamlines in the vicinity of the chain. The results on shape factor (λ) and average Nusselt Number (Nu) have been reported over the range of parameters considered in the present work. Finally, the functional dependence of drag correction factor λ and Nu on Reynolds number (Re) and number of spheres in the chain (N) have been established by simple expressions to facilitate interpolation to intermediate values of Re and N to enable a priori estimation in a new application.</p>
18.	<p>Generalizations of some concentration inequalities MA Bhat, GSR Kosuru - <i>Statistics & Probability Letters</i>, 2022</p> <p>Abstract: For a real-valued measurable function f and a nonnegative, nondecreasing function ϕ, we first obtain a Chebyshev type inequality which provides an upper bound for $\phi(\lambda_1)\mu(\{x \in \Omega: f(x) \geq \lambda_1\}) + \sum_{k=2}^n \phi(\lambda_k) - \phi(\lambda_{k-1})\mu(\{x \in \Omega: f(x) \geq \lambda_k\})$, where $0 < \lambda_1 < \lambda_2 < \dots < \lambda_n < \infty$. Using this, generalizations of a few concentration inequalities such as Markov, reverse Markov, Bienaymé–Chebyshev, Cantelli and Hoeffding inequalities are obtained.</p>
19.	<p>Improving Surface Characteristics and Corrosion Resistance of Medical Grade 316L by Titanium Powder Mixed Electro-Discharge Treatment G Singh, M Singh, SS Sidhu, TR Ablyaz - <i>Surface Topography: Metrology and Properties</i>, 2022</p> <p>Abstract: The article focuses on the corrosion behavior of medical grade 316L stainless steel used in cardiac stents, orthopaedic, and dental implants. In this research work, electro-discharge treatment (EDT) was used for the deposition of titanium dioxide (TiO₂) particles on 316L stainless steel to improve its corrosion-resistant property. The samples were characterized using scanning electron microscopy and x-ray diffraction techniques to correlate the modified surface with the EDT process parameters. The electrochemical corrosion analysis shows a lower corrosion rate for the TiO₂ coated specimen (1.883 mpy) compared to the untreated surface (13.729 mpy). This improved corrosion resistance of TiO₂ coated substrate was attributed to the formation of various silicides, carbides, and bioactive compounds.</p>
20.	<p>Integrated Power Converter with G2V and V2G capabilities for 4-Phase SRM Drive Based EV Application V Shah, S Payami - <i>2nd International Conference on Smart Technologies for Power, Energy and Control</i>, 2021</p> <p>Abstract: The article presents an integrated power converter (IPC) for EV (electric vehicle) application employing 4-phase switched reluctance machine (SRM) drive. In the discussed IPC an improved miller converter, and a bidirectional converter reconfigured on-board battery charger/discharger is integrated. During driving mode, an improved miller converter is reconfigured from the IPC, and the battery energy storage system (BESS) supplies driving power for SRM. When EV is in idle condition, the employed IPC is reconfigured as a cascade connection of bidirectional DC-DC and bidirectional AC-DC converter, performing two functions. (1) During battery charging, i.e., grid-to-vehicle (G2V), the bidirectional AC-DC converter exhibit characteristics of a single-phase bridgeless boost power factor correction circuit (PFCC). The buck type DC-DC converter in cascade achieves constant current/ constant voltage charging of BESS. (2) During battery discharging, i.e., vehicle-to-grid (V2G), the boost type DC-DC converter boosts the BESS voltage. And the bidirectional AC-DC converter exhibit characteristics of a single-phase voltage source inverter (VSI). For realizing the charging inductors during G2V/V2G charging, 4-phase SRM phase windings are used. Thus, the proposed</p>

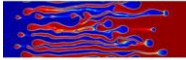
	<p>IPC without any off-board circuit is capable of charging/discharging BESS at AC grid voltage. Also, the control technique ensures zero net torque production during the charging/discharging process.</p>
21.	<p>Investigation into Hydrogen-Induced Blister Cracking and Mechanical Failure in Pipeline Steels V Singh, KS Arora, DK Mahajan - <i>Advances in Structural Integrity: Part of the Lecture Notes in Mechanical Engineering</i> book series, 2022</p> <p>Abstract: This work aims to investigate the role of hydrogen-induced blisters on tensile and fatigue damage of pipeline steels (X65 and X80). The electrochemical method of hydrogen charging is employed to simulate hydrogen-induced blister formation. Similar hydrogen charging conditions resulted in different sizes, shapes, and numbers of blisters in both types of steels. DIC analysis coupled with in-situ tensile testing confirmed the blisters as potential stress concentration sites. Synergistic action of hydrogen and stress concentration around these blister-type notches intensified the overall mechanical damage of material under the hydrogen atmosphere. The size and relative position of blisters are significant factors to degrade the mechanical performance of investigated pipeline steels.</p>
22.	<p>Investigation of bifurcations in cyclic combustion dynamics of a CNG-diesel RCCI engine A Singh, MR Saxena, RK Maurya - <i>Fuel</i>, 2022</p> <p>Abstract: This study uses nonlinear dynamical and chaotic methods to investigate the cyclic combustion dynamics of a CNG-Diesel reactivity control compression ignition (RCCI) engine. The experiments of RCCI combustion mode are conducted on a single-cylinder automotive diesel engine with the development ECU. Low reactivity fuel (i.e., CNG) is injected into the intake manifold, and high reactivity fuel (i.e., diesel) is injected directly into the engine cylinder during the RCCI experiments. Mass of fuel injection per cycle and their injection events are controlled by using ECU. The engine is tested for fixed engine load and speed of 3 bar BMEP and 1500 rpm, respectively. A double diesel injection strategy is used for injecting the diesel fuel into the engine cylinder. In-cylinder pressure is measured using a piezoelectric pressure transducer on a crank angle basis with a resolution of 0.1 CAD. Combustion parameters are calculated on a cyclic basis from measured in-cylinder pressure. In this study, the effect of diesel injection timing (SOI-2) on the behavior of combustion dynamics for two different masses of port-injected CNG fuel (mc) is investigated. The CA50 time series of 1000 consecutive engine cycles is analyzed for combustion dynamics analysis using symbol sequence analysis, return maps, recurrence plots (RPs), recurrence quantitative analysis (RQA), and 0–1 test. The peaks in symbol sequence histograms and the corresponding symbol series depict the period-2 nature of the cyclic combustion dynamics at the intermediate SOI-2 of 30° and 40° bTDC. Return maps also confirm the onset of noisy period-2 bifurcation at 30° bTDC SOI-2. The dominance of deterministic period-2 characteristics is found in the cyclic combustion dynamics at 30° and 40° bTDC SOI-2 using recurrence plots. The 0–1 test method depicts stronger chaotic cyclic combustion dynamics at 20° and 50° bTDC SOI-2. In summary, the present study supports the existence of a periodic window in between the chaotic combustion for the intermediate values of SOI-2. The dominance of the deterministic characteristics makes this regime of intermediate SOI-2 values suitable for a better cycle resolved control.</p>
23.	<p>Janus Aluminum Oxysulfide Al₂OS: A promising 2D direct semiconductor photocatalyst with strong visible light harvesting Z Haman, N Khossossi, M Kibbou, I Bouziani... R Ahuja - <i>Applied Surface Science</i>, 2022</p> <p>Abstract: Hydrogen production via solar light-driven water dissociation has been regarded as an</p>

	<p>artificial and effective process to overcome the environmental problem as well as solving the current energy crisis. In this regard, numerous works have mainly been devoted to developing the appropriate photocatalyst which satisfies the conditions for water splitting and understanding the photocatalysis process. In this study, we propose for the first time the potential application of the two-dimensional Janus aluminum oxysulfide Al₂OS as an efficient photocatalyst material for hydrogen-production H₂ through the first-principles calculations. Janus Al₂OS monolayer has been designed from the parental binary aluminum sulfide AlS by substituting one sub-layer of sulfide atoms (S) to oxygen atoms (O). The electronic properties of the pristine AlS and the derived Janus Al₂OS were computed using GGA-PBE and HSE06 functionals. According to the band structure, AlS monolayer shows a semiconductor behavior with an indirect bandgap of 2.14 eV whereas, the Janus Al₂OS exhibits a direct bandgap of 1.579 eV. Motivated by the desirable bandgap of the Janus Al₂OS, the absorption-coefficient of Janus Al₂OS shows strong visible light harvesting compared to the parental AlS. Furthermore, the photocatalytic performance of Al₂OS has been investigated. Our calculations demonstrate that the band edge position of Al₂OS is suitable for the hydrogen evolution reaction (HER). More importantly, based on the reaction coordinate, it was found that the Gibbs free-energy ΔGH^* of Al₂OS is 0.97 eV which is smaller than of the two-dimensional Janus Ga₂XY (X, Y = S, Se, Te with X \neq Y) reported recently. Moreover, this value decreases from 0.97 eV to 0.69 eV under 0.5 V/Å of an external electrical field. Our results indicate that Janus Al₂OS fulfills the fundamental requirements for efficient photo-catalyst under visible light and provides new guidance for hydrogen-production via water splitting.</p>
24.	<p>Large-scale mRNA translation and the intricate effects of competition for the finite pool of ribosomes A Jain, M Margaliot, AK Gupta - Journal of The Royal Society Interface, 2021</p> <p>Abstract: We present a new theoretical framework for large-scale mRNA translation using a network of models called the ribosome flow model with Langmuir kinetics (RFMLK), interconnected via a pool of free ribosomes. The input to each RFMLK depends on the pool density, and it affects the initiation rate and the internal ribosome entry rates at each site along each RFMLK. Ribosomes that detach from an RFMLK due to termination or premature drop-off are fed back into the pool. We prove that the network always converges to a steady-state, and study its sensitivity to variations in the parameters. For example, we show that if the drop-off rate at some site in some RFMLK is increased then the pool density increases and consequently the steady-state production rate in all the other RFMLKs increases. Surprisingly, we also show that modifying a parameter of a certain RFMLK can lead to arbitrary effects on the densities along the modified RFMLK, depending on the parameters in the entire network. We conclude that the competition for shared resources generates an indirect and intricate web of mutual effects between the mRNA molecules, that must be accounted for in any analysis of translation.</p>
25.	<p>MTGLS: Multi-Task Gaze Estimation with Limited Supervision S Ghosh, M Hayat, A Dhall... - Proceedings of the IEEE/CVF Winter Conference on Applications of Computer Vision, 2022</p> <p>Abstract: Robust gaze estimation is a challenging task, even for deep CNNs, due to the non-availability of large-scale labeled data. Moreover, gaze annotation is a time-consuming process and requires specialized hardware setups. We propose MTGLS: a Multi-Task Gaze estimation framework with Limited Supervision, which leverages abundantly available non-annotated facial image data. MTGLS distills knowledge from off-the-shelf facial image analysis models, and learns strong feature representations of human eyes, guided by three complementary auxiliary signals: (a) the line of sight of the pupil (i.e. pseudo-gaze) defined by the localized facial</p>

	<p>landmarks, (b) the head-pose given by Euler angles, and (c) the orientation of the eye patch (left/right eye). To overcome inherent noise in the supervisory signals, MTGLS further incorporates a noise distribution modelling approach. Our experimental results show that MTGLS learns highly generalized representations which consistently perform well on a range of datasets. Our proposed framework outperforms the unsupervised state-of-the-art on CAVE (by approx. 6.43%) and even supervised state-of-the-art methods on Gaze360 (by approx. 6.59%) datasets.</p>
26.	<p>Multifunctional cobalt iron sulfide electrocatalyst for high performance Zn-air battery and overall water splitting M Kumar, TC Nagaiah - Journal of Materials Chemistry A, 2022</p> <p>Abstract: Developing a highly efficient, inexpensive, and robust catalyst with multifunctional activity is pivotal and central to regenerative greener metal–air batteries and fuel cells. However, it is still a big challenge to achieve the integration of three functions in a single catalyst. Herein, we report a facile, template-free and scalable strategy to synthesize nanorod embedded wheat-grain CoFe(3:1)S₂ in conjunction with nitrogen-containing carbon by a simple single-step hydrothermal reaction. The synthesized catalyst demonstrates remarkable pH-universal hydrogen evolution activity and requires only 98, 117, and 123 mV overpotential in 0.5 M H₂SO₄, 1 M KOH and 1 M PBS to achieve a current density of 10 mA cm⁻². The optimized catalyst also exhibits a remarkable bifunctional oxygen activity and when CoFe(3:1)S₂ is used as an air cathode, it demonstrates a very high peak power density of 387 mW cm⁻² and energy density of 1008 W h kg⁻¹ with prolonged cycling stability. Besides, a water electrolyzer assembled using a CoFe(3:1)S₂ based anode and cathode affords a current density of 10 mA cm⁻² at a low cell potential of 1.584 V. When two Zn–air batteries are connected in series, they successfully powered overall water splitting, manifesting the feasibility of CoFe(3:1)S₂ for various energy conversion and storage systems.</p>
27.	<p>Natural Convection from a Confined Sphere in Yield stress Fluids S Nalluri, P Suri, SA Patel, RP Chhabra - Proceedings of the 26th National and 4th International ISHMT-ASTFE Heat and Mass Transfer Conference, 2021</p> <p>Abstract: Laminar natural convection in a yield stress fluid filled in the annular region between two concentric spheres with a constant heat flux condition on the inner sphere and an isothermal temperature on the outer sphere was investigated numerically. The numerical results presented here span a wide range of parameters, Rayleigh number ($10^2 \leq Ra \leq 10^6$), Prandtl number ($30 \leq Pr \leq 100$) and Bingham number ($0 \leq Bn \leq Bn_{max}$) illustrating the momentum and heat transfer characteristics in the steady regime. The effect of confinement has been investigated by varying the annular gap (gap ratio, $B = \text{inner sphere diameter, } D_i / \text{outer sphere diameter, } D_o$) from 0.1-0.5. The finite element based numerical study shows that there exists a critical Bingham number (or yield stress) for each confinement beyond that fluid motion completely ceases and heat transfer occurs by conduction only. The critical Bingham number is strongly influenced by the values of B and it increases with Ra. The present results also confirm that beyond the critical Bingham number, heat transfer is governed solely by conduction where the average Nusselt number attains a constant limiting value dependent on B only. A dimensionless criterion in terms of $Bn \times Pr^{1/2}$ corresponding to the onset of the conduction limit has been established over the range of parameters. The results of yielded-unyielded zones, isotherms and streamlines have been analysed below the critical yield stress limit. Finally, the functional dependence of the average Nusselt number has been established for each confinement in terms of Rayleigh number, Prandtl number and Bingham number embraced in this work.</p>

28.	<p>Nature of seniority symmetry breaking in the semimagic nucleus ^{94}Ru B Das, B Cederwall, C Qi, M Górska, PH Regan... A Sharma... - Physical Review C, 2022</p> <p>Abstract: Direct lifetime measurements via γ-γ coincidences using a fast timing detector array consisting of $\text{LaBr}_3(\text{Ce})$ scintillators has been applied to determine the lifetime of low-lying states in the semimagic ($N=50$) nucleus ^{94}Ru. The experiment was carried out as the first in a series of “FAIR-0” experiments with the DESPEC experimental setup at the Facility for Antiproton and Ion Research (FAIR). Excited states in ^{94}Ru were populated primarily via the β-delayed proton emission of ^{95}Pd nuclei, produced in the projectile fragmentation of an 850 MeV/nucleon ^{124}Xe beam impinging on a 4 g/cm^2 ^9Be target. While the deduced E2 strength for the $2^+ \rightarrow 0^+$ transition in the yrast cascade follows the expected behavior for conserved seniority symmetry, the intermediate $4^+ \rightarrow 2^+$ transition exhibits a drastic enhancement of transition strength in comparison with pure-seniority model predictions as well as standard shell model predictions in the fpg proton hole space with respect to doubly magic ^{100}Sn. The anomalous behavior is ascribed to a subtle interference between the wave function of the lowest seniority $\nu=2$, $I^\pi=4^+$ state and that of a close-lying $\nu=4$ state that exhibits partial dynamic symmetry. In addition, the observed strongly prohibitive $6^+ \rightarrow 4^+$ transition can be attributed to the same mechanism but with a destructive interference. It is noted that such effects may provide stringent tests of the nucleon-nucleon interactions employed in state-of-the-art theoretical model calculations.</p>
29.	<p>Numerical Analysis of a Flat Plate Solar Collector Integrated with Porous Copper Foam V Kulkarni, AS Kashyap, M Pal, H Tyagi - Proceedings of the 26th National and 4th International ISHMT-ASTFE Heat and Mass Transfer Conference, 2021</p> <p>Abstract: As a possible alternative to limited fossil fuels, renewable energy such as solar has stood out as an ideal candidate. Commonly, the flat plate collector, is used to harness solar energy, but it has limitations such as inherent thermal resistance, deterioration of selective surface, and inefficient heat dissipation. Recent studies corroborate the merit of porous material in improving the performance of a flat-plate collector. The porous material by virtue of its structural arrangement provides an additional surface area within the limited volume. In addition, the interconnected tortuous path provided to working fluid, facilitates in improving thermal mixing and heat transfer.</p> <p>In this paper, a numerical study of a flat plate collector integrated with porous copper foam is presented. The influence of the height of the porous foam, Darcy number (Da) and volumetric flow rate (V) on the performance is resented. The optimum configuration is obtained when $S = 1$, where highest enhancement in Nusselt number (Nu) and bulk outlet temperature is obtained. Further, the numerical results also show lucrative improvement in Nu of about 5.7 % and 8.8 % with decrease in Da from 10^{-2} to 10^{-6} and increase in V from 0.25 L/min to 1 L/min.</p>
30.	<p>Numerical Investigation of Buoyancy-assisted and-opposed flows in the Laminar Regime of Mixed Convection through a Vertical Channel S Gorai, D Samanta, SK Das - Proceedings of the 26th National and 4th International ISHMT-ASTFE Heat and Mass Transfer Conference, 2021</p> <p>Abstract: The present study focused on simultaneously hydrodynamically and thermally developing regime of laminar mixed convection for the investigation. Numerical simulations of buoyancy- aiding and -opposing flow have been performed to understand the heat transfer, pressure drop and flow characteristics of air in a vertical channel subjected to uniform heat flux from the side walls. Two-dimensional steady state simulations are performed in ANSYS-Fluent for a length-to-width (L/H) ratio of 50. The structured mesh was generated with uniform grids in axial and non-uniform in transverse directions. The effects of Reynolds number ($100 \leq Re \leq$</p>

	<p>2300), Grashof number ($10^3 \leq Gr \leq 5.29 * 10^5$) on fluid flow and heat transfer respectively are studied. The corresponding range of Richardson number (Ri) is 1 to 1.5. In case of assisting flow, it has been observed that the velocity is accelerated near the wall compared to the center of the channel. In contrast, velocity is accelerated at the center as compared to the wall in case of opposing flow. The pressure drops as well as heat transfer is higher in assisting flow as that of the opposing flow for a fixed Ri and Re. Further, it has been inferred from the results that the hydrodynamic and thermal entry length are dependent on Gr.</p>
31.	<p>Numerical Simulation of Latent Heat Thermal Energy Storage Incorporated Solar Water Heater AS Kashyap, H Tyagi - Proceedings of the 26th National and 4th International ISHMT-ASTFE Heat and Mass Transfer Conference, 2021</p> <p>Abstract: As the global energy demand is increasing [1], storing energy is found to be one of the major challenges of today's era. Thermal energy storage (TES) is considered to be very significant among the various forms of energy storage, because of its ability to store and releasing energy in the form of cold or heat [2]. Among the different TES forms, latent heat thermal energy storage (LHTES) is found to be highly effective as it stores high energy amount at a nearly constant temperature when phase change occurs [3]. This ability of LHTES makes it applicable to solar energy systems using phase change materials (PCMs). The intermittency associated with solar energy is a major restriction for its continuous usage, which can be dealt with using TES. The surplus solar energy can be converted into thermal energy and stored in a PCM, and discharged whenever the energy demand occurs. The application of PCM in a flat plate collector is focused in this present study. In this study, a numerical simulation is done for a solar water heater (SWH) with a shell-and-tube PCM storage unit by using the CFD tool ANSYS.</p>
32.	<p>Numerical Study of Methanol Steam Reformation in a Micro-Solar Thermal Collector for Producing Hydrogen G Gupta, H Tyagi - Proceedings of the 26th National and 4th International ISHMT-ASTFE Heat and Mass Transfer Conference, 2021</p> <p>Abstract: Power generation systems should be made portable and miniaturized to fulfil power demands while traveling or in remote areas. Fuel cells provide a portable, clean, and efficient way of power generation. But one of the challenges associated with it is the safety issue associated with the hydrogen. In this regards, methanol is quite safe for in-situ production of hydrogen. Methanol steam reformation (MSR) yields high percentage of hydrogen. For MSR to take place, around 200-300°C of temperature is required, which can be achieved by using solar energy. In this study, a flat-plate solar collector is used with selective surface coating and vacuum layers on either side of the absorber, in order to produce hydrogen. A stagnation study shows that a temperature of 350°C could be achieved. A numerical model is set up using ANSYS software to simulate the heat transfer process and the reformation reaction taking place inside the microchannels. The thermal efficiency of the collector is found to be 48.4% with incident heat flux of 1000W/m². The process parameter study of the reformation reaction shows that at flow rate of 5mL/h and reformation temperature of 250°C, the optimum results are obtained, for the parameters considered in this study. The product contains approximately 63% of H₂ with only 1.8% of CO. This hydrogen-rich product could be used in PEMFCs (Proton-exchange membrane fuel cell) to produce electricity.</p>
33.	<p>Numerical study on topological change of viscous fingering induced by a phase separation with Korteweg force S Seya, RX Suzuki, Y Nagatsu, T Ban, M Mishra - Journal of Fluid Mechanics, 2022</p>

	<p>Abstract: We develop coupled evolution equations for viscous fingering (VF) and phase separation in partially miscible systems by combining a simple double-well thermodynamic free energy and Korteweg force with a classical miscible VF model for a binary system. The VF pattern transition into a droplet formation pattern by the spinodal decomposition effect is demonstrated, and the simultaneous increases in the depth of the energy minimum, in the difference in the equilibrium concentrations, and in the Korteweg force, enhance the droplet growth. The pattern's interfacial length increases with the spinodal decomposition effects. These results match the corresponding experimental results.</p> 
34.	<p>On a conjecture of Murty–Saradha about digamma values T Chatterjee, S Dhillon - Monatshefte für Mathematik, 2022</p> <p>Abstract: The arithmetic nature of the Euler’s constant γ is one of the biggest unsolved problems in number theory from almost three centuries. In an attempt to give a partial answer to the arithmetic nature of γ, Murty and Saradha made a conjecture on linear independence of digamma values. In particular, they conjectured that for any positive integer $q > 1$ and a field K over which the q-th cyclotomic polynomial is irreducible, the digamma values namely $\psi(a/q)$ where $1 \leq a \leq q$ with $(a,q)=1$ are linearly independent over K. Further, they established a connection between the arithmetic nature of the Euler’s constant γ to the above conjecture. In this article, we first prove that the conjecture is true with at most one exceptional q. Later on we also make some remarks on the linear independence of these digamma values with the arithmetic nature of the Euler’s constant γ.</p>
35.	<p>Parametric Study of Hybrid Vapour Absorption Refrigeration System (VARS) with Humidification-Dehumidification (HDH) Desalination R Beniwal, K Garg, H Tyagi - Proceedings of the 26th National and 4th International ISHMT-ASTFE Heat and Mass Transfer Conference, 2021</p> <p>Abstract: The demand for air conditioning and freshwater is increasing at a rapid pace due to urbanization and climate change. This rising demand is met mainly by using conventional sources of energy, i.e. coal and oil. As these are highly energy-intensive processes, it is imperative to shift towards use of renewable energy sources (such as solar energy). This paper presents the study of solar energy-based hybrid single-effect ammonia-water based vapour absorption refrigeration system (VARS) coupled with humidificationdehumidification (HDH) desalination technique for simultaneous air conditioning and freshwater production. The cooled water picks the heat rejected by the VARS system, and this heated water is used as the feed for the humidifier of the HDH system. A mathematical model is prepared for this hybrid VARS-HDH cycle. Two different configurations (Case I and Case II) for utilization of the heat rejected by the VARS system are considered. The mass flow rate of the distillate produce and the Gain Output Ratio (GOR) of the system have been analyzed in detail, based on variation in parameters such as mass flow rate of water to the inlet of humidifier, mass flow rate of water through the dehumidifier, mass flow rate ratio and temperature of water at the dehumidifier inlet.</p>
36.	<p>Particle creation and annihilation in an exclusion process on networks A Gupta, AK Gupta - Journal of Physics A: Mathematical and Theoretical, 2022</p>

	<p>Abstract: To mimic the complex transport-like collective phenomena in a man-made or natural system, we study an open network junction model of totally asymmetric simple exclusion process with bulk particle attachment and detachment. The stationary system properties such as particle density, phase transitions, and phase diagrams are derived theoretically utilising the mean field approach. The steady-state phases have been categorized into various sub-classes based upon the phase transitions occurring across the junction. It is found that the number of steady-state phases depends on the number of incoming and outgoing segments at the junction. Further, an increase in the particle non-conserving rates significantly affects the topology of the phase diagram, and the number of stationary phases changes in a non-monotonic way. For both the case of equal and unequal incoming and outgoing segments, the critical values of non-conserving rates at which the topology of the phase diagram changes are identified. The theoretical results are validated using extensive Monte Carlo simulations.</p>
37.	<p>Platinum nanoparticle sensitized plasmonic-enhanced broad spectral photodetection in large area vertical-aligned MoS2 flakes R Wadhwa, A Ghosh, D Kumar, P Kumar, M Kumar - Nanotechnology, 2022</p> <p>Abstract: 2D MoS2 holds immense potential for electronic and optoelectronic applications due to its unique characteristics. However, the atomic-scale thickness of MoS2 hinders the optical absorbance, thereby limiting its photodetection capability. Vertically-aligned MoS2 (VA-MoS2) has an advantage of strong optical absorption and quick intra-layer transport, offering high speed operation. The coupling of plasmonic metal nanostructure with MoS2 can further enhance the light-matter interaction. Pt/Pd (as opposed to Ag/Au) are more promising to design next-generation nano-plasmonic devices due to their intense interband activity over a broad spectral range. Herein, we report Pt nanoparticle (NPs) enhanced broadband photoresponse in VA-MoS2. The optical absorbance of MoS2 is enhanced after the integration of Pt NPs, with a four-fold enhancement in photocurrent. The formation of Schottky junction at Pt-MoS2 interface inhibits electron transmission, suppressing the dark current and substantially reducing NEP. The plasmonic-enabled photodetector shows enhanced responsivity (432 AW⁻¹, 800 nm) and detectivity (1.85 × 10¹⁴ Jones, 5 V) with a low response time (87 ms /84 ms), attributed to faster carrier transport. Additionally, a theoretical approach is adopted to calculate wavelength-dependent responsivity, which matches well with experimental results. These findings offer a facile approach to modulate the performance of next-generation optoelectronic devices for practical applications.</p>
38.	<p>Puzzle on isomeric configurations in and around N = 126 closed shell B Maheshwari, D Choudhury, AK Jain – Physical Review C, 2022</p> <p>Abstract: The puzzle of finding consistent nuclear configurations to explain both the decay probabilities and moments of the 9/2⁻, 8⁺, and 21/2⁻ isomers in and around the N=126 closed shell has been approached in the generalized seniority scheme. Though h_{9/2} is the dominant orbital near Fermi energy, the role of configuration mixing from the surrounding f_{7/2} and i_{13/2} orbitals is found to be very important for the consistent explanation of all the isomeric properties such as the B(E2) rates, Qmoments, and g factors. The structural behavior of the closed shell N=126 isotonic isomers turns out to be very similar to that of the N=124 and N=128 isotonic isomers, which have two neutron holes and two neutron particles, respectively. This is due to the pairing symmetries of nuclear many-body Hamiltonian. As confirmation, the microscopic shell model occupancies are also calculated for these isomers in the N=126 chain which support the generalized seniority results. Additional arguments using the systematics of odd-proton 9/2⁻ states in Tl (Z=81), Bi (Z=83), At (Z=85), and Fr (Z=87) isotopes are also presented.</p>

[Real-Time scheduling on Hierarchical Heterogeneous Fog Networks](#)

A Kaur, N Auluck, O Rana - IEEE Transactions on Services Computing, 2022

39. **Abstract:** Cloud computing is widely used to support offloaded data processing for applications. However, latency constrained data processing has requirements that may not always be suitable for cloud-based processing. Fog computing brings processing closer to data generation sources, by reducing propagation and data transfer delays. It is a viable alternative for processing tasks with real-time requirements. We propose a scheduling algorithm RTH2S (Real Time Heterogeneous Hierarchical Scheduling) for a set of real-time tasks on a heterogeneous integrated fog-cloud architecture. We consider a hierarchical model for fog nodes, with nodes at higher tiers having greater computational capacity than nodes at lower tiers, though with greater latency from data generation sources. Tasks with various profiles have been considered. For regular profile jobs, we use least laxity first (LLF) to find the preferred fog node for scheduling. For tagged profiles, based on tag values, the jobs are split in order to finish execution before the deadline, or the LLF heuristic is used. Using HPC2N workload traces across 3.5 years of activity, the real-time performance of RTH2S versus comparable algorithms is demonstrated. Our proposed approach is validated using both simulation (to demonstrate scale up) as well as a lab-based testbed.

[Recycling of Ti6Al4V machining swarf into additive manufacturing feedstock powder to realise sustainable recycling goals](#)

S Dhiman, RS Joshi, S Singh, SS Gill, H Singh... - Journal of Cleaner Production, 2022

40. **Abstract:** This paper addresses the imperative need to develop sustainable recycle technologies for high value machining swarf generated during the processing of Ti6Al4V alloy. A novel recycling process based on multi-stage ball milling is proposed. The process converts Ti6Al4V swarf into a powder feedstock suitable for additive manufacturing (AM). The powders produced from the cleaned swarf using an in-house designed and fabricated tumbler ball mill were characterised in terms of their morphology, particle size, flowability and spreadability. It was found that the dominant effect of milling with \varnothing 25 mm balls was particle size reduction (up to \sim 40%) and the primary effect with smaller balls of \varnothing 6.25 mm was modification of particle morphology from irregular to rounded shape; thus, necessitating adoption of a multi-stage milling approach to achieve required size and morphology. Ti6Al4V powder having particle size in the range of 40–200 μ m and near-spherical morphology was obtained after multi-stage ball milling up to 18 h. The powder characteristics were comparable or superior to the powder produced by generally used gas atomization (GA) process. The suitability of the powders for AM was established through direct metal laser sintering (DMLS). The proper melting of the optimally prepared powder occurs at 1000 mm/s scanning speed and 310 W of laser power. The developed multi-stage ball milling process was assessed vis-à-vis gas atomization using life cycle assessment (LCA). LCA revealed that the proposed ball milling method consumed lower energy (\sim 59%), had lower eco-cost (\sim 82%), and lesser global warming potential (GWP) (\sim 68%).

Graphical Abstract:



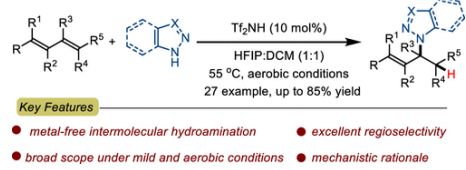
41. [Redox-active Alkylsulfones as a Precursor for Alkyl Radicals under Photoredox Catalysis](#)
I Chatterjee, S Patel, B Paul, H Paul, R Shankhdhar - Chemical Communications, 2022

	<p>Abstract: A method for generating alkyl radicals using visible-light photoredox catalysis is described. This procedure was found to present an efficient means to access a diverse collection of 1°, 2°, and 3° alkyl radicals through the single-electron transfer of sulfones under mild reaction conditions. These alkyl radicals generated via the reductive desulfonylation of readily synthesized and stable alkylsulfones were engaged to forge C–C bonds. A detailed study was also carried out to shed light on the mechanism.</p>
42.	<p>Revealing the superlative electrochemical properties of o-B₂N₂ monolayer in Lithium/Sodium-ion batteries N Khossossi, W Luo, Z Haman, D Singh, I Essaoudi... R Ahuja - Nano Energy, 2022</p> <p>Abstract: Promising flexible electrochemical energy storage systems (EESSs) are currently drawing considerable attention for their tremendous prospective end-use in portable self-powered electronic devices, including roll-up displays, and “smart” garments outfitted with piezoelectric patches to harvest energy from body movement. However, the lack of suitable battery electrodes that provides a specific electrochemical performance has made further development of these technologies challenging. Two-dimensional (2D) lightweight and flexible materials with outstanding physical and chemical properties, including mechanical strengths, hydrophilic surfaces, high surface metal diffusivity, and good conductivity, have been identified as a potential prospect for battery electrodes. In this study, taking a new 2D boron nitride allotrope, namely 2D orthorhombic diboron dinitride monolayer (o-B₂N₂) as representatives, we systematically explored several influencing factors, including electronic, mechanical, and their electrochemical properties (e.g., binding strength, ionic mobility, equilibrium voltage, and theoretical capacity). Considering potential charge-transfer polarization, we employed a charged electrode model to simulate ionic mobility and found ionic mobility has a unique dependence on the surface atomic configuration influenced by bond length, valence electron number, electrical conductivity, excellent ionic mobility, low equilibrium voltage with excellent stability, good flexibility, and extremely superior theoretical capacity, up to 8.7 times higher than that of widely commercialized graphite (3239.74 mAh g⁻¹ Vs 372 mAh g⁻¹) in case of Li-ion batteries and 2159.83 mAh g⁻¹ in case of Na-ion batteries, indicating that the new predicted 2D o-B₂N₂ monolayer possess the capability to be ideal flexible anode materials for Lithium and Sodium-ion battery. Our finding provides valuable insights for experimental explorations of flexible anode candidates based on 2D o-B₂N₂ monolayer.</p>
43.	<p>Scattering of oblique water waves by thick porous structure and thin elastic plate G Sahoo, S Singla, SC Martha - Ocean Engineering, 2022</p> <p>Abstract: The present study deals with the usefulness of the partial porous structure of finite width placed at a finite distance from the elastic plate to mitigate the hydrodynamic response of the elastic plate. Two different configurations of the porous structure namely bottom-standing and surface-piercing structures are analyzed. The elastic plate is modeled using thin plate theory, and the wave past the thick porous structure is based on Sollitt and Cross model, the problems are investigated based on the small-amplitude water wave theory in water of finite depth. With the aid of the eigenfunction expansion method, the associated boundary value problem is reduced to a system of linear algebraic equations, which is solved numerically. For both configurations, the effects of various system parameters such as wavenumber and angle of incidence are analyzed. The impacts of structural parameters such as length, width of the porous structure, porosity are investigated from the graphs plotted on the reflection coefficient, transmission coefficient and dissipation coefficient and hydrodynamic forces. Further, detailed analysis on free surface elevation, elastic plate deflection, shear force and strain is presented. The study reveals that with</p>

	<p>an increase in length, width, porosity, and friction factor of the porous structure the dissipation of wave energy increases which helps in diminishing the wave impact on the elastic plate.</p>
44.	<p>SDCN2: A Shallow Densely connected CNN for multi-purpose image manipulation detection G Singh, P Goyal - ACM Transactions on Multimedia Computing, Communications, and Applications Accepted on January 2022 https://doi.org/10.1145/3510462, 2022</p> <p>Abstract: The digital image information can be easily tampered to harm the integrity of someone. Thus, recognizing the truthfulness and processing history of an image is one of the essential concerns in multimedia forensics. Numerous forensic methods have been developed by researchers with the ability to detect targeted editing operations. But, creating a unified forensic approach capable of detecting multiple image manipulations is still a challenging problem. In this paper, a new general-purpose forensic approach is designed based on a shallow densely connected CNN (SDCN2) that exploits local dense connections and global residual learning. The residual domain is considered in the proposed network rather than the spatial domain to analyze the image manipulation artifacts because the residual domain is less dependent on image content information. To attain this purpose, a residual convolutional layer is employed at the beginning of the proposed model to adaptively learn the image manipulation features by suppressing the image content information. Then, the obtained image residuals or prediction error features are further processed by the shallow densely connected CNN for high-level feature extraction. Also, the hierarchical features produced by the densely connected blocks (DCBs) and prediction error features are fused globally for better information flow across the network. The extensive experiment results show that the proposed scheme outperforms the existing state-of-the-art general-purpose forensic schemes even under anti-forensic attacks, when tested on large scale datasets. The proposed model offers overall detection accuracies of 98.34% and 99.22% for BOSSBase and Dresden datasets, respectively for multiple image manipulation detection. Moreover, the proposed network is highly efficient in terms of computational complexity as compared to the existing approaches.</p>
45.	<p>Simulation studies for source optimization in $^{96}\text{Zr}\beta$ decay S Thakur, V Nanal, PP Singh, RG Pillay, H Krishnamoorthy, A Mazumdar, A Reza, PK Raina, V Vatsa - Nuovo Cimento della Societa Italiana di Fisica C, 2022</p> <p>Abstract: The single β decay of ^{96}Zr to the ground state of ^{96}Nb is spin forbidden and poses a great experimental challenge. The β decay of ^{96}Zr can be studied via coincident detection of de-exciting gamma rays in ^{96}Mo, which is the end product of ^{96}Nb β decay. Simulations are done with four high purity Ge (HPGe) detector setup ($\sim 33\%$ relative efficiency each) to optimize the source configuration. The results suggest that ~ 70 g of 50% enriched ^{96}Zr will yield sensitivity comparable to the reported results.</p>
46.	<p>The Impact of Neutron Transfer Reactions on the Heating and Cooling of Accreted Neutron Star Crusts H Schatz, Z Meisel, EF Brown, SS Gupta... - The Astrophysical Journal, 2022</p> <p>Abstract: Nuclear reactions heat and cool the crust of accreting neutron stars and need to be understood to interpret observations of X-ray bursts and long-term cooling in transiently accreting systems. It was recently suggested that previously ignored neutron transfer reactions may play a significant role in the nuclear processes. We present results from full nuclear network calculations that now include these reactions and determine their impact on crust composition, crust impurity, heating, and cooling. We find that a large number of neutron transfer reactions indeed occur and impact crust models. In particular, we identify a new type of reaction cycle that brings a pair of nuclei across the nuclear chart into equilibrium via alternating neutron capture and neutron</p>

	<p>release, interspersed with a neutron transfer. While neutron transfer reactions lead to changes in crust model predictions and need to be considered in future studies, previous conclusions concerning heating, cooling, and compositional evolution are remarkably robust.</p>
47.	<p>Thermal and photocatalytic cascade one-pot synthesis of secondary amine using multifunctional Pd decorated MOF-derived CeO₂ GS More, N Kushwaha, R Bal, R Srivastava - Journal of Colloid and Interface Science, 2022</p> <p>Abstract: The use of a single catalyst to perform thermal and photochemical N-alkylation of amine is challenging work. Herein, Pd decorated MOF-derived CeO₂ was prepared for the cascade one-pot synthesis of secondary amine by thermal and photocatalytic routes. Among the designed catalysts, Pd(0.5%)/CeO₂-300 exhibited the best activity for thermal and photocatalytic one-pot secondary amine synthesis involving benzyl alcohol and aniline. The physicochemical characteristics of Pd(0.5%)/CeO₂-300 suited for the oxidation of benzyl alcohol followed by condensation with aniline to form an imine. Further, reduction of imine over Pd NPs decorated on CeO₂-300 took place to form secondary amine. An excellent conversion of benzyl alcohol and secondary amine selectivity was observed thermally at 100 °C in 26 h. The Pd(0.5%)/CeO₂-300 exhibited excellent activity in white LED. Interestingly, more activity was achieved in sunlight. The Pd(0.5%)/CeO₂-300 demonstrated excellent stability under thermal and photocatalytic conditions and was recycled 5 times without losing any significant activity. The surface area, acidity, and elemental compositions were characterized by various physicochemical techniques. The light absorption property, bandgap, charge carrier separation, and photocurrent measurements were carried out by photoelectrochemical and optoelectronic analysis. The reaction mechanism and structural activity relationship correlated with control experiments, catalytic activity data, physicochemical, and optoelectronic characterization. One catalyst affording efficient activity in conventional thermal and photocatalytic conditions, especially sunlight, would be exciting to researchers and industrial practitioners.</p>
48.	<p>Thermal-Aware Modeling and Analysis of Cu-Mixed CNT Nanocomposite Interconnects B Kumari, S Pandrangi, R Sharma, M Sahoo - IEEE Transactions on Nanotechnology, 2022</p> <p>Abstract: Growing only single-walled carbon nanotube or only multi-walled carbon nanotube in a bundle is not feasible practically. Thus, a random number of SWCNTs and MWCNTs whose diameters are also varied randomly (following a Gaussian distribution) should be considered in a bundle of mixed carbon nanotubes. A thermal aware electrical modeling of copper-mixed carbon nanotube (Cu-MCNT) composite interconnects is proposed here and its performance and reliability have been studied and compared with copper interconnect at 7 nm and 11 nm technology nodes. It is observed that an increase in filling fraction (FMCNT) of mixed carbon nanotube in Cu-MCNT composites leads to a decrease in delay. But in some cases, if the fraction of SWCNT is greater than that of MWCNT in a bundle, then it leads to a higher delay. Variation in delay with respect to FMCNT is more at higher temperature by 10%. Cu-MCNT composite interconnects with FMCNT = 0:5 have 52% higher breakdown power than copper interconnects and are thermally more efficient as evident from the temperature profiles. It is found that fabrication efforts to further improve FMCNT are not needed because the improvement in performance and reliability saturates for (FMCNT > 0.5). Scaling down the dimensions leads to degradation in performance and reliability combined but this degradation is more in copper interconnect when compared to Cu-MCNT composite interconnect by 14% which makes it even more suitable for scaled technology requirements. Cu-MCNT composite interconnects attain 39% less temperature rise at steady state when compared to copper interconnects. The performance of Cu-MCNT composite interconnects in terms of meantime to failure at high current densities is phenomenal as compared to copper interconnects. Our study promotes Cu-MCNT composite</p>

	interconnects as an alternate candidate to copper interconnect considering their superior electrothermal performances.
49.	<p>Thermodynamic activity of a ternary nanofluid flow passing through a permeable slipped surface with heat source and sink GK Ramesh, JK Madhukesh, R Das, NA Shah, SJ Yook - Waves in Random and Complex Media, 2022</p> <p>Abstract: Interaction of nanoparticles with fluids is receiving considerable interest in the area of nanotechnology research. The purpose of this research is to see how a ternary nanofluid performs over a slippery surface. The energy equation is used to explain the heat source/sink effect. As a novel feature of the article, suction, slip effect, and convective boundary conditions are incorporated at the wall. The physical flow problem is formulated using boundary layer equations, which are then transformed into dimensionless forms by employing appropriate variables. Using the RKF-45 approach and the shooting operation, numerical solutions of transmuted equations are obtained. The proposed framework was validated against the available data and found to be relatively accurate. Investigation confesses that enhanced values of the suction parameter decelerate the temperature, whereas slip, Biot number and heat source/sink parameter accelerate the temperature. Further, ternary nanofluid shows a high rate of thermal distribution than hybrid and mano nanofluid. These results reflect a diverse range of practical applications, such as transportation cooling, petroleum resource recovery, wastewater disposal, thermal insulation, and geothermal systems.</p>
50.	<p>Thermodynamics Analysis of an Atmospheric Water Harvesting System T Singh, R Beniwal, K Garg, H Tyagi - Proceedings of the 26th National and 4th International ISHMT-ASTFE Heat and Mass Transfer Conference, 2021</p> <p>Abstract: A numerical study of harvesting water from the air was performed. The system also uses a humidifier with water sourced from wastewater or available saline water and thus incorporates wastewater management simultaneously. The heat required for the regeneration of the desiccant can be taken from some low-grade energy source or from solar energy. The system was mathematically defined and solved using the MATLAB software to analyze the variation of input parameters such as Dry Bulb Temperature (DBT), Relative Humidity (RH), the inlet temperature of the desiccant, the Mass Flow Ratio (MFR) of desiccant to air are varied, and their effect on the system performance was observed. The results obtained by the thermodynamic analysis of the proposed Atmospheric Water Harvesting (AWH) system show that about 3.8 kgh-1 of water can be extracted from the air at ambient conditions of 40°C DBT and 40% RH. The results show that AWH systems can be used to generate new sources of water in arid regions also.</p>
51.	<p>Transition-Metal-Free Regioselective Intermolecular Hydroamination of Conjugated 1, 3-Dienes with Heterocyclic Amines S Pradhan, S Das, G Kumar, I Chatterjee - Organic Letters, 2022</p> <p>Abstract: The unique property of hexafluoroisopropanol (HFIP) enables the regioselective hydroamination of 1,3-dienes with nitrogen heterocycles in a Markovnikov manner in the presence of catalytic Brønsted acid. This transition-metal-free intermolecular hydroamination protocol is achieved under mild reaction conditions. The aggregation by HFIP and Brønsted acid helps to activate the terminal double bond regioselectively. Following the protonation of diene, the C–N bond formation is accomplished upon the involvement of heterocyclic amines.</p>

	 <p>Key Features</p> <ul style="list-style-type: none"> ● metal-free intermolecular hydroamination ● excellent regioselectivity ● broad scope under mild and aerobic conditions ● mechanistic rationale
52.	<p>Understanding Users Attitude towards Information Technology Application in University Libraries T Singh, J Singh - DESIDOC Journal of Library & Information Technology, 2022</p> <p>Abstract: In the present study, researchers aim to understand the attitude of users towards information technology application in two university libraries of north India, namely Himachal Pradesh University, Shimla and Panjabi University, Patiala. Survey method of research was used to collect data from the users. The sample consisted of 391 users, which included PG Students, Research Scholars and Faculty Members in the Faculties of Social Sciences and Sciences in both the universities. The data were collected through structured questionnaires and further analysed using the Chi-Square test and Kruskal-Wallis test. The data analysis and discussion reveals that despite a few number of library users being involved in the decision-making of IT application in libraries and availability of few training programmes on the know-how of IT systems, a positive attitude towards information technology application prevails among the library users in both the university libraries. In the end, some key recommendations are presented for deriving more benefits from future IT initiatives in libraries.</p>
53.	<p>Wall Energy Loss and Entropy Generation in Solar Ponds using One-Dimensional and Two-Dimensional Transient Analyses S Verma, R Das - Journal of Energy Resources Technology, 2022</p> <p>Abstract: In this paper, wall thermal energy loss in a cylindrical solar pond is studied using one-dimensional (1D) and two-dimensional (2D) transient models. It is seen that for a given quantity of insulation applied around the pond wall, the negative effect of sidewall loss reduces as the pond size increases. Further, the optimal insulation thickness that eradicates all wall energy loss is larger when calculated from a spatially 1D model, as opposed to when radial temperature gradients are given consideration. The 2D model reveals a larger entropy generation than that calculated by a 1D model for an imperfectly insulated pond. So, for such ponds, the present model would calculate entropy generation in a more realistic manner. It is revealed that using simpler 1D in space models to estimate solar pond's outer wall optimum insulation thickness will not lead to any problems as far as the thermal performance is the concern. But, since such models over predict the optimum value, they would invoke more cost. So, when financial and space constraints are present, then it is advisable to design the wall insulation in solar ponds using spatially multi-dimensional heat transfer models, for which the present work could prove to be useful.</p>

Disclaimer: This publication digest may not contain all the papers published. Library has compiled the publication data as per the alerts received from Scopus and Google Scholar for the affiliation "Indian Institute of Technology Ropar" for the month of March 2022. The author(s) are requested to share their missing paper(s) details if any, for the inclusion in the next publication digest.